International Symposium
On Turbulence and Shear Flow
Phenomena (TSFP-8)
August 28 - 30, 2013 Poitiers, France

DNS ON MULTISCALE-GENERATED GRID TURBULENCE USING A CLASSICAL GRID

Hiroki Suzuki
Department of Mechanical Engineering
Nagoya Institute of Technology
Gokiso-cho, Showa-ku, Nagoya, Japan
hsuzuki@nitech.ac.jp

Kouji Nagata
Department of Mechanical Science
and Engineering
Nagoya University
Furo-cho, Chikusa-ku, Nagoya, Japan
nagata@nagoya-u.jp

Yasuhiko Sakai
Department of Mechanical Science
and Engineering
Nagoya University
Furo-cho, Chikusa-ku, Nagoya, Japan
ysakai@mech.nagoya-u.ac.jp

Toshiyuki Hayase
Institute of Fluid Science
Tohoku University
Katahira, Aoba-ku, Sendai, Japan
hayase@ifs.tohoku.ac.jp

Yutaka Hasegawa
Department of Mechanical Engineering
Nagoya Institute of Technology
Gokiso-cho, Showa-ku, Nagoya, Japan
hasegawa.yutaka@nitech.ac.jp

Tatsuo Ushijima
Department of Mechanical Engineering
Nagoya Institute of Technology
Gokiso-cho, Showa-ku, Nagoya, Japan
ushijima@nitech.ac.jp

ABSTRACT

We carry out direct numerical simulation of experimental grid turbulence, for which the mesh Reynolds number is 2500. The grid is directly constructed in the computational domain. The streamwise computational domain size is >100 times the mesh size. The value of the decay exponent n is estimated as $n \approx 1.36$ by using a ratio defined by the turbulent kinetic energy and its dissipation. The prevailing perspective is that the memory of the turbulence cannot be considered as short. In this paper, we propose a promoter that focuses on the generation of turbulence using the grid, not on the shape of the grid, as addressed in previous studies (Hurst & Vassilicos (2007); Krogstad & Davidson (2011)), from a multiscale perspective and investigate the effects of the turbulence-generating method on the decay exponent n. Specifically, n is increased to $n \approx 1.53$ and 1.41 because of the changes in the initial conditions.

INTRODUCTION

Grid turbulence is the most fundamental type of turbulent flow and has been studied extensively (Pope (2000)). Grid turbulence usually becomes highly homogeneous in the downstream region (Hinze (1975)). Its decay follows a power law, which includes a decay coefficient, the virtual origin, and the decay exponent (Mohamed & LaRue (1990); Pope (2000)) applicable in the region. The decay exponent is directly related to the fundamental characteristics of the decaying grid turbulence. If the grid turbulence is modeled by the Saffman turbulence (Hinze (1975)), the decay exponent will be close to $6/5$ (Krogstad & Davidson (2010)) when the turbulent Reynolds number is sufficiently high.

Mohamed & LaRue (1990) proposed a method in which a search is performed for the fit that gives the smallest variance between the data and the form of the decay power law. Wang & George (2002) proposed an indirect means of obtaining the power law through the Taylor microscale. In this work, we employ another method to estimate the decay exponent and the virtual origin by focusing on a principal relation in grid turbulence.

Wakes produced by the grid are significantly affected by the grid configuration (Mohamed & LaRue (1990); Lavoie *et al.* (2005)). The prevailing perspective is that the memory of the generated turbulence cannot be considered to be short (Davidson (2004)). In addition, scatter of the decay exponent among experiments may reflect the dependence of the decay exponent on initial conditions (George (1992)).

In recent previous studies (mainly Hurst & Vassilicos (2007)), the turbulence generated by using a grid of a specific fractal shape has been investigated. However, in these previous studies, the concept of multiscale generation of turbulence was added to the generation of turbulence by focusing on the shape of the grid, not on the generation of turbulence by the grid. In this paper, we propose a promoter that focuses on the generation of turbulence using the grid, not on the shape of the grid, and we investigate the effects of the initial conditions on the decay exponent of grid turbulence.

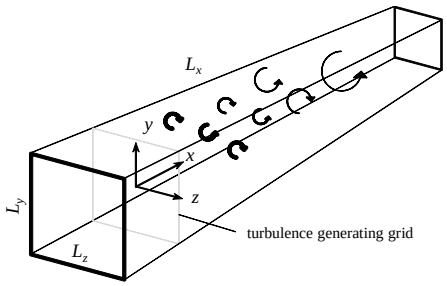

Figure 1. Schematic of the computational domain and the coordinate system.

CLASSICAL GRID TURBULENCE

Numerical simulation

The turbulence-generating grid used in this study is a biplanar grid composed of rectangular bars; the solidity σ of the grid is 0.36. Therefore, the ratio between the mesh size $M\,[\mathrm{m}]$ and the width of the square bars $d\,[\mathrm{m}]$, M/d, is exactly 5. This is a useful value because most of the grids used for turbulence investigations also have $M/d \approx 5$ (Hinze (1975)). The chosen value of σ is also similar to that used in previous experiments (for example, Mohamed & LaRue (1990)). Note that the physical length of the mesh size M does not need to be set in this simulation because the mesh size is a characteristic length of the mesh Reynolds number Re_M, defined as $\mathrm{Re}_M \equiv U_o M/\nu$, where $U_o\,[\mathrm{m/s}]$ is a uniform inflow velocity used as the characteristic velocity and $\nu\,[\mathrm{m^2/s}]$ is the kinematic viscosity.

In this simulation, Re_M is set to be 2500. Although this value is smaller than those of previous experiments (mainly, Comte-Bellot & Corrsin (1966); Mohamed & LaRue (1990); Lavoie *et al.* (2007); Krogstad & Davidson (2010)), it is similar to those of a previous experiment (Kurian & Fransson (2009)).

A schematic of the computational domain size and coordinate system is shown in Figure 1. Computational domain size, which is normalized by the mesh size, is $L_x \times L_y \times L_z = 112 \times 8 \times 8$, and grid points are $N_x \times N_y \times N_z = 2304 \times 160 \times 160$. We also carried out a simulation under $N_x \times N_y \times N_z = 2304 \times 256 \times 256$ using the same size computational domain and confirmed that there are hardly any differences in results between these. In previous experiments, the value of L_y is set to be larger than that of the present value. The integral length scale increases in the streamwise direction and has a value similar to that of the mesh size at $(x/M)/\mathrm{Re}_M = 100/2500$ regardless of Re_M (Kurian & Fransson (2009)). Thus, the ratio between $L_y(=L_z)$ and the integral length scale at $x/M = 100$ is about 8. This value is similar to or is larger than those obtained in previous direct numerical simulation (DNS) works (Jiménez *et al.* (1993); Kaneda *et al.* (2003)). Note that the side walls of the wind tunnel have no effect in this simulation because a periodic condition is applied to cross-sectional directions in contrast to the experiments.

For the governing equations, we used the incompressible continuity equation and the Navier–Stokes (N-S) equations:

$$\frac{\partial \tilde{u}_i}{\partial x_i} = 0, \tag{1}$$

$$\frac{\partial \tilde{u}_i}{\partial t} + \frac{\partial \tilde{u}_i \tilde{u}_j}{\partial x_j} = -\frac{\partial p}{\partial x_i} + \frac{1}{\mathrm{Re}_M}\frac{\partial^2 \tilde{u}_i}{\partial x_j \partial x_j} + F_i, \tag{2}$$

where the nondimensional parameter included in the above governing equation is the mesh Reynolds number Re_M.

The inflow boundary condition is the uniform flow condition. At the exit, we applied a convective outflow condition, in which the convective velocity at the exit is set to be the cross-sectional-averaged free-stream velocity, whose normalized value is exactly unity. A biplaner grid was numerically constructed by using the force term in the N-S equation.

A fractional step method, based on a third-order Runge–Kutta method, was applied for solving the governing equations. The spatial derivatives of the continuity equation terms and the nonlinear terms in the N-S equations were discretized by using a fourth-order central difference scheme (Morinishi *et al.* (1998)). The Poisson equation, which must be solved for each fractional step, was solved by using a direct solver based on a two-dimensional fast Fourier transform and a matrix algorithm directly. Therefore, a high level of mass conservation was realized. Because of this and the introduction of the discretization scheme of Morinishi *et al.* (1998), conservation of turbulent kinetic energy (so-called secondary conservation) was highly maintained in our simulation. Specifically, the accuracy of the secondary conservation is of the third order in the time increment, which is the same order as that of the Runge–Kutta scheme. In this simulation, by setting a fine grid system around the grid to avoid incidences of numerical instability, no numerical viscosity or filtering schemes had to be applied, thereby avoiding any potential erosion in the secondary conservation.

Because of the differences between the differential orders of the viscous terms and the other terms, a higher-order differential scheme would be effective for maintaining the spatial resolution of the viscous terms. Thus, the order of accuracy of the differential schemes used for the viscous terms was set to be higher than those for the other terms (Suzuki *et al.* (2013)), thus improving the accuracy of higher-order statistics and various spectra. Note that the increase in the required computational time will not be crucial when incompressible flow is simulated because the introduction of a higher-order scheme for the viscous terms does not increase the computational cost for solving the Poisson equation (Morinishi *et al.* (1998)).

Validation of present DNS results We examined the accuracy of the numerical construction for the turbulence-generating grid in terms of the pressure drop across the grid. Empirical laws for the pressure drop resulting from various turbulence-generating grids have been shown in a previous study (Roach (1987)). An empirical law for a square mesh of square bars is given as

$$\Delta P = 0.98(1/\beta^2 - 1)^{1.09}, \tag{3}$$

where ΔP is the pressure drop normalized by the inflow dynamic pressure and $\beta = 1 - \sigma$. ΔP estimated by using this empirical law is about 1.46. The present value of ΔP was about 1.54, so the relative difference between these is about 5.5%.

Results and discussion

Power-law decay of turbulent kinetic energy The flow field downstream of the turbulence-generating grid is separated into three regions. The first is the developing region behind the grid where wakes generated by the bars are sequenced; here, no section of the

flow is homogeneous and isotropic. Even if the grid is sufficiently spatially uniform, there will be inhomogeneities in the lateral direction of the flow, which may be due to wake instability (Hinze (1975)). The region of the final period of decay, in which large-scale eddies are directly affected by viscous effects, lies sufficiently far downstream from the grid.

Grid turbulence usually becomes highly homogeneous when $x/M > 10$–15 (Hinze (1975)). A decay power law form is applicable in the region between the first region and the region of the final period of decay (Mohamed & LaRue (1990)). Specifically, by using Taylor's hypothesis for conversion from time to downstream position, the normal stresses $\langle u^2\rangle, \langle v^2\rangle$, and $\langle w^2\rangle$ for the streamwise, lateral, and spanwise directions, respectively, and turbulent kinetic energy (TKE) $k = \frac{1}{2}(\langle u^2\rangle + \langle v^2\rangle + \langle w^2\rangle)$ decay as power laws, can be written as as

$$k = A(x/M - x_o/M)^{-n} = AX^{-n}, \tag{4}$$

where $\tilde{u} = U + u$, $U = \langle \tilde{u} \rangle$, $\langle\ \rangle$ denotes ensemble average. The normal stresses and the TKE are quantities normalized by the square of the free-stream velocity U_o. The above relation includes three constants: A is the decay coefficient, x_o is the virtual origin, and n is the decay exponent (Mohamed & LaRue (1990); Pope (2000)). Note that the decay coefficient is directly related to the pressure drop across the grid (Kistler & Vrebalovich (1966)). In particular, a relation $A \propto 1/C_D$ is proposed with a concept of the linear decay law, where C_D is the drag per unit area of the grid (Hinze (1975)). Indeed, A varies with the grid configuration (Mohamed & LaRue (1990)).

These three constants are usually estimated by fitting the relation to the measured profiles. Data near the grid, where the flow is inhomogeneous, anisotropic and the power-law decay is inapplicable, should not be used to determine the constants. In conventional grid turbulence for grids with a relatively low solidity, it is considered good practice to restrict to $x/M > 25$–40 to avoid the inhomogeneous region (Comte-Bellot & Corrsin (1966)). In fact, for example, measurements were taken at a far enough downstream location (Lavoie *et al.* (2007)). In another case, Mohamed & LaRue (1990) eliminated data at $x/M \leq 40$ in the estimation of the constants. This elimination is also applied to data when the mesh Reynolds number Re_M is low to moderate (Kurian & Fransson (2009)). The order of the critical streamwise point normalized by the mesh size would be insensitive to the value of Re_M (Kurian & Fransson (2009)).

In the grid turbulence field obtained by using the present DNS, the following characteristics are evident (Fig. 2): The constancy of k/X^{-n} in the streamwise direction indicates that the form of the decay power law is applicable only in the downstream region. The value of the normalized critical streamwise point is about 60, which agrees with previous estimated values (Kurian & Fransson (2009)) with similar Re_M quantitatively. It should be noted that the value of n is discussed in the next subsection because, generally, n can be a function of x_o/M even if the error of a least-squares fitting can be minimized (Mohamed & LaRue (1990)). The value of the virtual origin x_o/M in the figure is set to be $x_o/M = 4$, which is only provisional, in this estimation.

How to estimate n and x_o/M The decay exponent n is directly related to the fundamental characteristics of decaying grid turbulence. Most grid turbulence is well modeled not by the Batchelor turbulence but by the Saffman turbulence, as pointed out more than three decades ago (Hinze (1975)), so the value of n will be close to not $10/7$ but $6/5$ when the turbulent Reynolds number is high enough (Krogstad & Davidson (2010)).

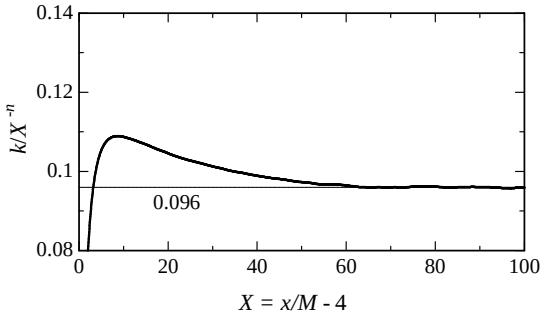

Figure 2. Streamwise profiles of k/X^{-n} in upstream and downstream regions, where n is the decay exponent.

As briefly mentioned above, there are three unknowns that must be determined in a least-squares fitting. Mohamed & LaRue (1990) proposed a method in which a search is performed for the fit that gives the smallest variance between the data and Eq. (4). They concluded that the root mean square values of the difference do not differ significantly for different values of the virtual origin. As a consequence, an estimated value of n depending on x_o/M is allowed (Mohamed & LaRue (1990)); therefore, they took the virtual origin to be zero. A method based on Mohamed & LaRue (1990)'s method is applied to fit the form of the decay power law to the data from recent experiments (Krogstad & Davidson (2010, 2011); Kurian & Fransson (2009)).

Wang & George (2002) proposed an indirect means of obtaining the power law through the Taylor microscale λ, for which

$$\frac{d\lambda^2}{dt} = \frac{10}{nU}\frac{1}{\mathrm{Re}_M}, \tag{5}$$

where the relation is a normalized formula, and, in contrast to the method applied by Mohamed & LaRue (1990), n is only included in the relation to the fit. This method was applied to estimate the decay exponent of decaying turbulence found in previous DNS works (Jiménez *et al.* (1993); de Bruyn Kops & Riley (1998)). Unfortunately, however, it may not be practical to use this relation owing to significant noise (Lavoie *et al.* (2007)).

In this work, we apply another way to estimate n and x_o/M. A principal relation in grid turbulence in the downstream region is as follows:

$$\frac{dk}{dt} = U\frac{dk}{dX} = -\varepsilon. \tag{6}$$

By also applying $k = AX^{-n}$ and $U = 1$ in the downstream region, we obtain

$$k/\varepsilon = X/n = (x/M - x_o/M)/n. \tag{7}$$

Therefore, n and x_o/M are estimated by fitting Eq. (7) to the data set. The main difference between these methods lies in the number of unknowns.

In this work, indeed, there are a region where k/ε increases linearly downstream (Fig. 3). By fitting Eq. (7), n and x_o/M are estimated as

$$n \approx 1.36 \text{ and } x_o/M \approx 4.93. \tag{8}$$

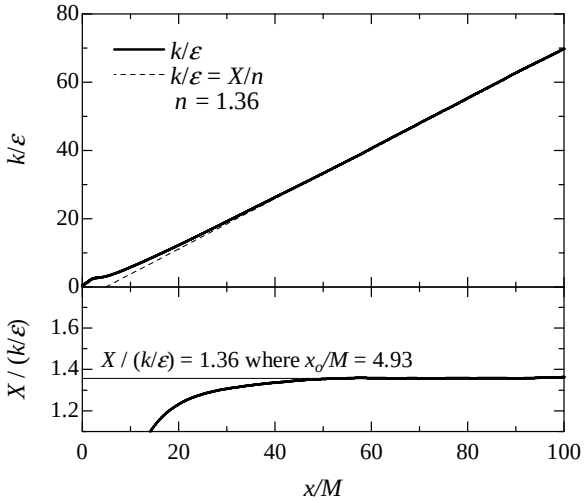

Figure 3. Streamwise profiles of k/ε (the upper figure) and $X/(k/\varepsilon)$ (the lower figure), where $X = x/M - x_o/M$.

Decay exponent of TKE The N-S equation turns out to have a constant turbulent Reynolds number as an invariant, implying a decay exponent of unity, which is expected from dimensional analysis and is the so-called linear decay law. Early experimental results seem to support the prediction that $n = 1$ (for example, Kistler & Vrebalovich (1966)). However, later experiments (mainly Comte-Bellot & Corrsin (1966); Mohamed & LaRue (1990)) led to $n > 1$. In particular, the value of n varies between 1.2 and 1.35 in most experiments, with the average value of $n \approx 1.25$ being close to the theoretical prediction of Saffman turbulence (Hinze (1975)). In fact, the invariant of grid turbulence may be that of Saffman turbulence (Krogstad & Davidson (2010)).

The estimated value of n in the grid turbulence field is about 1.36 (the lower panel of Fig. 3) and is slightly larger than those obtained in previous experiments (mainly Comte-Bellot & Corrsin (1966); Mohamed & LaRue (1990); Krogstad & Davidson (2010)). There is a possibility that n increases as Re_M decreases (Kurian & Fransson (2009)). The present value qualitatively agrees with this tendency. Note that the present grid turbulence does not result in the final period of decay, because the present value is sufficiently smaller than $5/2$, which is the decay exponent in this stage.

One may note that the present value is slightly larger than that of the Saffman turbulence. However, this difference is not significant if the present grid turbulence is not modeled by Saffman turbulence, because n may be affected by varying the dissipation constant in the streamwise direction (Krogstad & Davidson (2010)). The exponent of the integral scale is also needed to discuss characteristics of the invariant.

MULTISCALE-GENERATED GRID TURBULENCE

A promoter for multiscale-generated turbulence

Wakes produced by the grid are significantly affected by the grid configuration of the turbulence-generating grid (Mohamed & LaRue (1990)). For instance, round-rod grids produce more periodic structures than square-bar grids

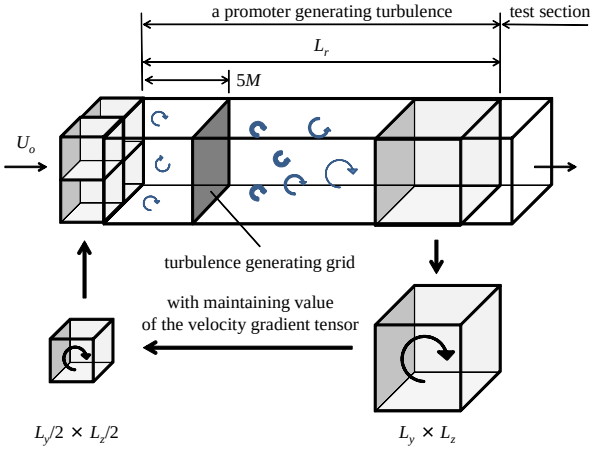

Figure 4. Schematic of the inflow conditions for the promoter used for multiscale-generated turbulence.

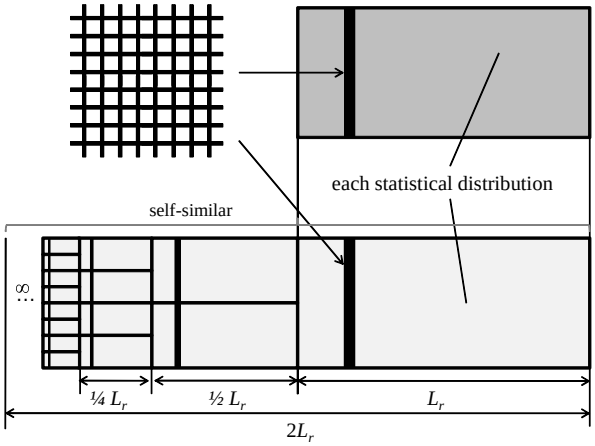

Figure 5. Schematics showing a comparison between a classical grid and the promoter used for multiscale-generated turbulence.

(Lavoie *et al.* (2005)). Although it is often considered that turbulence has a short memory, there is a possibility that this perspective need not be true (Davidson (2004)).

Varying values of the decay exponent n have been obtained in most of the previous experiments (Hinze (1975)). This scatter may reflect the dependence of the decay exponent on initial conditions, i.e., on how turbulence was produced (George (1992)). Different grid geometries produce variations of the decay exponent and affect the structure of turbulence (Lavoie *et al.* (2005)). The effects of initial conditions on n are being experimentally investigated in grid turbulence (Lavoie *et al.* (2005)), in which only the shape of the bars are changed. In contrast, there is one conclusion that n is insensitive to various initial conditions and only the decay coefficient A is mainly affected by the grid configuration (Mohamed & LaRue (1990)).

The relation between the shape of a turbulence-generating grid and the turbulence generated by it has been studied (Mohamed & LaRue (1990); Lavoie *et al.* (2007); Hurst & Vassilicos (2007); Krogstad & Davidson (2011)). Previous studies (Hurst & Vassilicos (2007); Mazellier & Vassilicos (2010); Valente & Vassilicos (2011); Krogstad & Davidson (2011)) have been performed to investigate the turbulence generated using a grid of a specific frac-

Table 1. Numerical conditions. Run CG is the same as for the previous grid turbulence. σ is the solidity of the largest grid. Krogstad & Davidson (2011) and Hurst & Vassilicos (2007) are referred to as KD (2011) and HV (2007), respectively.

	Grid	N	σ
Run CG	CG	–	0.36
Run MG1	MG ($L_r = 10$)	∞	0.36
Run MG2	MG ($L_r = 20$)	∞	0.36
KD (2011)	CG	–	0.36
KD (2011)	MG of HV (2007)	3	0.23, 0.17

tal shape (MG, hereinafter); such turbulence is often referred to as fractal-generated turbulence (Hurst & Vassilicos (2007)). In particular, the fractal-generated turbulence generated by using the square-type fractal grid proposed by Hurst & Vassilicos (2007) has been studied by other researchers (mainly Mazellier & Vassilicos (2010); Valente & Vassilicos (2011)).

However, in the previous studies, the concept of multiscale generation of turbulence was added to the generation of turbulence focusing on the shape of the grid, not on the generation of turbulence by the grid. In this work, we propose a promoter that focuses on the generation of turbulence using the grid, not on the shape of the grid. Then, we numerically investigate a series of grid turbulence generated by a promoter based on the concept proposed in this study.

We attempt to add the concept to classical grid turbulence, shown in the previous section, by only changing the inflow boundary condition to be

$$\tilde{u_i}\left(-5, \frac{y}{2} \pm \frac{hL_y}{2}, \frac{z}{2} \pm \frac{hL_z}{2}\right) = \frac{1}{2}\tilde{u_i}(L_r - 5, y, z) \qquad (9)$$

while maintaining the value of the velocity gradient tensor. Figure 4 shows a schematic of the inflow boundary conditions for the promoter used for multiscale generation of grid turbulence. The concept of this multiscale-generated grid turbulence has been inspired by the recycling method for turbulent boundary layer of Lund *et al.* (1998).

By processing our calculations until grid turbulence is fully developed, virtually, we considered the multiscale-generated grid turbulence to have been generated. Figure 5 shows schematics comparing classical grid turbulence and multiscale-generated grid turbulence; the upper part of this figure shows the classical grid turbulence and the lower part shows the grid turbulence generated by the proposed promoter. Iteration number N (Hurst & Vassilicos (2007)) of the promoter is sufficiently large. The streamwise size of the promoter is exactly $2L_r$ because $L_r(1+1/2+1/2^2+\cdots) = L_r/(1-1/2) = 2L_r$.

Numerical simulation

The governing equations, numerical techniques, and numerical conditions such as grid points are the same as those of the classical grid turbulence shown in the previous section. The turbulence-generating grid is also the same. L_r is set to be $L_r = 10$ or 20 (referred to as Run MG1 and Run MG2, respectively). Run CG is a run for a classical grid turbulence (CG). Table 1 lists the numerical conditions of the

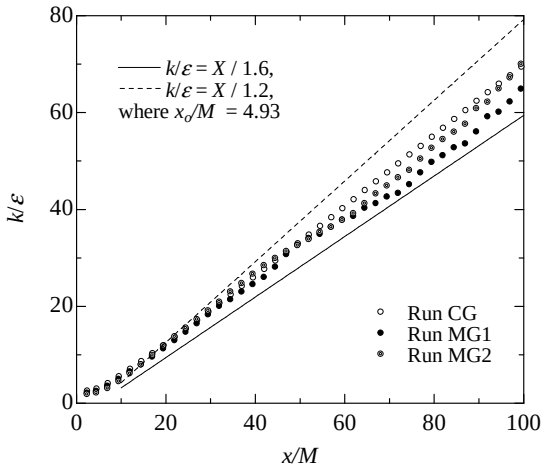

Figure 6. Comparison of the streamwise profile of k/ε between the classical and multiscale-generated grid turbulence cases.

Table 2. Values of the decay exponent and the virtual origin.

Run ID	n of k	x_0/M
Run CG	≈ 1.36	≈ 4.93
Run MG1	≈ 1.53	≈ 1.96
Run MG2	≈ 1.41	≈ 3.80

present runs for the multiscale-generated grid turbulence, compared with those of a previous experiment (Krogstad & Davidson (2011)). It should be noted that the turbulence-generating method of Krogstad & Davidson (2011) is not the same as that of our simulation. $t_r^{1/(N-1)} = d_l/d_{l+1} = 2$, where t_r is defined as the ratio of the largest and the smallest values of d (Hurst & Vassilicos (2007)), and l is number of each stage.

Results and discussion

Effects on the decay exponent of TKE

Figure 6 shows the streamwise profile of k/ε, for which the gradient is $1/n$ (see Eq. (7)). The linearly increasing profiles of the multiscale-generated grid turbulence indicate that the TKE still follows a power law decay.

Lines for two n values ($n = 1.2$ and 1.6) are also drawn in the figure. As shown in the figure, the multiscale-generated grid turbulence profiles for k/ε are closer for $n = 1.6$, but not for $n = 1.2$, implying that n is increasingly affected by changed initial conditions. Specific values of n, estimated in the region of $x/M > 30$, are listed in Table 2. As listed in the table, values of the virtual origin are also slightly changed.

The increase in the decay exponent resulting from changed initial conditions has also been investigated in previous experiments (Krogstad & Davidson (2011)) in which the turbulence-generating grid used is a cross grid (Hurst & Vassilicos (2007)) and for another experiment (Kurian & Fransson (2009)) with a similar Re_M value. Figure 7 compares the present results of the decay exponent with those of Kurian & Fransson (2009) and Krogstad & Davidson (2011), where those of Krogstad & Davidson (2011) in the

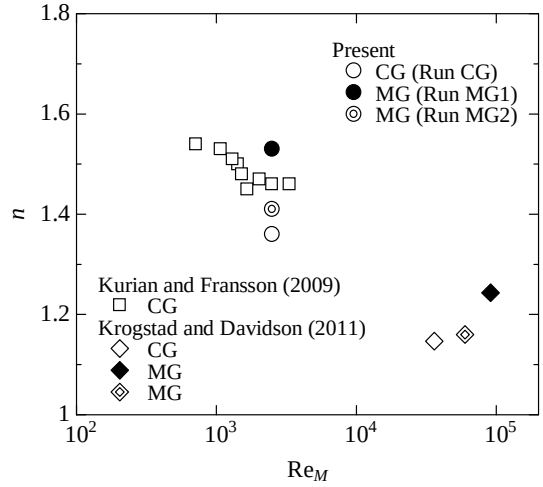

Figure 7. Comparison of the decay exponent n between the present DNS and previous experiments (Kurian & Fransson (2009); Krogstad & Davidson (2011)).

figure are averaged value over three methods to estimate n (see Krogstad & Davidson (2011)). As shown in the figure, the increase in the present decay exponent because of the change in initial conditions agrees with that of Krogstad & Davidson (2011) qualitatively. Although the largest grid of the present DNS, which is a grid of the first stage of grid generation, see Fig.5, is similar to that used in previous work, there are some differences in flow conditions and grid configurations (such as Re_M, N, and σ (Table 1)) and in the turbulence-generating method. Thus, further investigations and discussion will be needed to clarify the effects of initial conditions on the increase in n to $n \approx 1.53$ and 1.41.

CONCLUSION

We carried out direct numerical simulation of grid turbulence, for which the mesh Reynolds number is 2500. The value of the decay exponent n and virtual origin x_o/M were estimated as $n \approx 1.36$ and $x_o/M \approx 4.93$, respectively, by using a time scale defined by using turbulent kinetic energy and its dissipation. Then, we proposed a promoter to generate grid turbulence from a multiscale perspective and investigated the effects of our turbulence-generating method on the decay exponent n. The value of n was found to increase owing to changes in the initial conditions.

Acknowledgments

Part of this study was carried out under the Collaborative Research Project of the Institute of Fluid Science, Tohoku University. A portion of this study was supported by Grants-in-Aid (Nos. 22360076, 22360077, 24760133, 25289030, and 25289031) from the Japanese Ministry of Education, Culture, Sports, Science and Technology.

REFERENCES

Comte-Bellot, G. & Corrsin, S. 1966 The use of a contraction to improve the isotropy of grid-generated turbulence. *Journal of Fluid Mechanics* **25** (4), 657–682.

Davidson, P. A. 2004 *Turbulence: An Introduction for Scientists and Engineers*. Oxford University Press.

de Bruyn Kops, S. M. & Riley, J. J. 1998 Direct numerical simulation of laboratory experiments in isotropic turbulence. *Physics of Fluids* **10** (9), 2125–2127.

George, W. K. 1992 The decay of homogeneous isotropic turbulence. *Physics of Fluids* **4** (7), 1492–1509.

Hinze, J. O. 1975 *Turbulence*. McGraw-Hill.

Hurst, D. & Vassilicos, J. C. 2007 Scalings and decay of fractal-generated turbulence. *Physics of Fluids* **19** (3), 035103.

Jiménez, J., Wray, A. A., Saffman, P. G. & Rogallo, R. S. 1993 The structure of intense vorticity in isotropic turbulence. *Journal of Fluid Mechanics* **255**, 65–90.

Kaneda, Y., Ishihara, T., Yokokawa, M., Itakura, K. & Uno, A. 2003 Energy dissipation rate and energy spectrum in high resolution direct numerical simulations of turbulence in a periodic box. *Physics of Fluids* **15** (2), L21–L24.

Kistler, A. L. & Vrebalovich, T. 1966 Grid turbulence at large Reynolds numbers. *Journal of Fluid Mechanics* **26**, 37–47.

Krogstad, P.-Å. & Davidson, P. A. 2010 Is grid turbulence Saffman turbulence? *Journal of Fluid Mechanics* **642**, 373–394.

Krogstad, P.-Å. & Davidson, P. A. 2011 Freely decaying, homogeneous turbulence generated by multi-scale grids. *Journal of Fluid Mechanics* **680**, 417–434.

Kurian, T. & Fransson, J. H. M. 2009 Grid-generated turbulence revisited. *Fluid Dynamics Research* **41** (2), 021403.

Lavoie, P., Burattini, P., Djenidi, L. & Antonia, R. A. 2005 Effect of initial conditions on decaying grid turbulence at low R_λ. *Experiments in Fluids* **39** (5), 865–874.

Lavoie, P., Djenidi, L. & Antonia, R. A. 2007 Effects of initial conditions in decaying turbulence generated by passive grids. *Journal of Fluid Mechanics* **585**, 395–420.

Lund, T. S., Wu, X. & Squires, K. D. 1998 Generation of Turbulent Inflow Data for Spatially-Developing Boundary Layer Simulations. *Journal of Computational Physics* **140** (2), 233–258.

Mazellier, N. & Vassilicos, J. C. 2010 Turbulence without Richardson-Kolmogorov cascade. *Physics of Fluids* **22**, 075101.

Mohamed, M. S. & LaRue, J. C. 1990 The decay power law in grid-generated turbulence. *Journal of Fluid Mechanics* **219**, 195–214.

Morinishi, Y., Lund, T. S., Vasilyev, V. & Moin, P. 1998 Fully Conservative Higher Order Finite Difference Schemes for Incompressible Flow. *Journal of Computational Physics* **143** (1), 90–124.

Pope, S. B. 2000 *Turbulent Flows*. Cambridge University Press.

Roach, P. E. 1987 The generation of nearly isotropic turbulence by means of grids. *International Journal of Heat and Fluid Flow* **8** (2), 82–92.

Suzuki, H., Nagata, K., Sakai, Y., Hayase, T., Hasegawa, Y., & Ushijima, T. 2013 An attempt to improve accuracy of higher-order statistics and spectra in direct numerical simulation of incompressible wall turbulence by using the compact schemes for viscous terms. *International Journal for Numerical Methods in Fluids* (in press).

Valente, P. C. & Vassilicos, J. C. 2011 The decay of turbulence generated by a class of multiscale grids. *Journal of Fluid Mechanics* **687**, 300–340.

Wang, H. & George, W. K. 2002 The integral scale in homogeneous isotropic turbulence. *Journal of Fluid Mechanics* **459**, 429–443.